



OPEN ACCESS

EDITED BY

Hao Zou,
Chengdu University of Technology,
China

EDITED BY

Zhiye Gao,
China University of Petroleum, Beijing,
China

Xiaoqi Wu,
Sinopec Petroleum Exploration and
Production Research Institute, China

*CORRESPONDENCE

Zhijun Qin,
zhijunqin_karamay@126.com

SPECIALTY SECTION

This article was submitted
to Economic Geology,
a section of the journal
Frontiers in Earth Science

RECEIVED 29 September 2022

ACCEPTED 31 October 2022

PUBLISHED 17 January 2023

CITATION

Qin Z, Tang Y, Chang Q, Liu C and Ren H
(2023), The characteristics and genetic
mechanisms of the Upper Permian
Shangwuerhe clastic reservoir in the
eastern Junggar Basin,
Northwest China.
Front. Earth Sci. 10:1057313.
doi: 10.3389/feart.2022.1057313

COPYRIGHT

© 2023 Qin, Tang, Chang, Liu and Ren.
This is an open-access article
distributed under the terms of the
[Creative Commons Attribution License
\(CC BY\)](https://creativecommons.org/licenses/by/4.0/). The use, distribution or
reproduction in other forums is
permitted, provided the original
author(s) and the copyright owner(s) are
credited and that the original
publication in this journal is cited, in
accordance with accepted academic
practice. No use, distribution or
reproduction is permitted which does
not comply with these terms.

The characteristics and genetic mechanisms of the Upper Permian Shangwuerhe clastic reservoir in the eastern Junggar Basin, Northwest China

Zhijun Qin^{1,2*}, Yong Tang², Qiusheng Chang², Chaowei Liu²
and Haijiao Ren²

¹China University of Petroleum (East China), Shandong, China, ²Research Institute of Exploration and Development, Xinjiang Oil Company, PetroChina, China

In this paper, the lithology, pore type, throat structure, and physical characteristics of the sandstone and conglomerate reservoirs of the Upper Permian Shangwuerhe Formation in the Fukang Sag of the Junggar Basin were analyzed through rock cast thin section, scanning electron microscopy, fluid inclusions, piezometric mercury, and porosity–permeability analysis. In addition, the reservoir densification mechanism and the genesis of deep effective reservoirs were discussed. The results show that the reservoir is dominated by lithic sandstone (or lithic sandstone conglomerate). The lithic fragments primarily comprise tuffaceous volcanic rocks, supported by grains and cemented by clay, carbonate, authigenic quartz, and laumontite. The reservoir properties are characterized by extra-low porosity and permeability, and the pore type is dominated by inter- and intragrain dissolved pores of lithic fragments, feldspar, and quartz. The pore connectivity is poor due to poorly sorted extra-fine throat channels. The tightness of the reservoir is due to the strong cementation of calcite, chlorite, montmorillonite, illite-montmorillonite mixed layer, authigenic quartz, and laumontite. Furthermore, the large amount of Ca²⁺ released by the hydration of tuff rock debris and intermediate–basic volcanic rock debris and the CO₂-rich thermal fluid from the deep layers cause the development of several calcites. The formation of several montmorillonites is mainly related to the alteration of filled volcanic ash, and the hydration of volcanic tuff material primarily causes the development of laumontite cementation. The dissolution of feldspar and various volcanic lithic fragments by acidic fluids triggers the physical improvement of the reservoir in the local section.

KEYWORDS

reservoir characteristics, genesis mechanism, Shangwuerhe formation, Fukang Sag, Junggar Basin

1 Introduction

Due to the rise in oil and gas exploration in the basin uplift areas and shallow layers, and the rapid advancement of drilling and development technologies, the petroleum exploration field shifted from tectonic reservoirs in uplift areas to lithologic reservoirs in the depression areas. Moreover, it moved from conventional petroleum systems to unconventional systems (i.e., tight and shale petroleum systems) and from shallow to deep petroleum reservoirs (Jia et al., 2007, 2016; He and Li, 2014; Du et al., 2016; Hou et al., 2021; Liu et al., 2021; Zhang et al., 2021; Li et al., 2022).

Entering deep depressions for “near-source petroleum exploration” has become an important direction for current oil and gas exploration. Therefore, depression areas are becoming important for current oil and gas exploration (Zhou, 2005; Zou et al., 2009; Zhi et al., 2012; Du et al., 2014; Gong et al., 2018; Yang and Zou, 2019). Based on this, significant breakthroughs were made in depression areas in the Junggar Basin, such as the Mahu and Shawan sags located in the western part of the basin (Figure 1) (Zhi et al., 2012; Du et al., 2019; Tang et al., 2019; Song et al., 2022; Yu et al., 2022; Zhang et al., 2022). However, as the largest prolific depression in the Junggar Basin, the hydrocarbon



FIGURE 1 Tectonic units in the Junggar Basin and the location of Fukang Sag (after Lian et al., 2011; Gong et al., 2019).

exploration in the Fukang Sag has not yielded any significant discoveries. This may be because previous hydrocarbon exploration in the area centered on the bulge around the perimeter of the sag (Zhang, 2011; Wang et al., 2013; Sun et al., 2016; Gong et al., 2017, 2019; Hu et al., 2020; Wu et al., 2020). The important discovery of “near-source exploration” in the prolific Mahu and Shawan sags demands that exploration targets change from uplift to depression areas in the Fukang Sag.

In 2020, Well KT1 in the Fukang Sag drilled a highly productive oil formation in the Upper Permian Shangwuerhe Formation (P_{3w}), revealing that the Fukang Sag has favorable potential for hydrocarbon exploration in deep reservoirs (He et al., 2021). However, as a new exploration area, the reservoir characteristics and formation mechanisms of the effective P_{3w} reservoir in the Fukang Sag are still unclear. Based on rock cast thin section, scanning electron microscopy (SEM), fluid inclusions, piezometric mercury analysis, and porosity–permeability analysis of the latest drilled cores in the Fukang Sag, the characteristics and genesis mechanism of the P_{3w} reservoir were discussed. The results provided a basis for the preferential selection of promising targets and sweet-spot areas in the Fukang Sag.

2 Geological setting

The Junggar Basin is an important component of the Central Asian Orogenic Belt, which is located at the intersection of the Siberian Plate, the Kazakhstan Plate, and the Tarim Plate. It is bordered by the Junggar Mountains to the north and the Tien Shan Mountains to the south, and multiple secondary depressions are developed in the basin (Guo et al., 2020; Tang et al., 2021; Wu et al., 2021).

The Junggar Basin is a complex superimposed basin with deposits from the Late Carboniferous to Quaternary periods (Zhao et al., 2014; Tang et al., 2019; Tang et al., 2021; Wu et al., 2021). During the Late Carboniferous to early Permian periods, a foreland basin was formed under Hercynian compressional tectonics (Guo et al., 2020; Zhang et al., 2020). Simultaneously, the orogenic belt was rapidly elevated and denuded during the land–continental collision process, which provided sufficient provenance for the later stratigraphic deposition (Zhao et al., 2014; Xu et al., 2019; Wu et al., 2021). The orogeny weakened, and the basin evolution entered the whole depression stage of the inland basin during the Middle and late Permian periods. Due to the subsidence of the basin, the sedimentary range gradually increased, and the Middle–Upper Permian strata were deposited, overlying the uplift area that separates the depressions. The Triassic has been characterized by lacustrine deposits formed by inherited unified depressions (Wu et al., 2012; Zhao et al., 2014; Xu et al., 2019; Zhao et al., 2020; Wu et al., 2021).

Summarily, the Middle and late Permian were transitional periods from fault depression to depression. During those periods, the sediment provenance sufficiently provided much sedimentary debris for the depression area, with a large deposition thickness and wide distribution (Zhao et al., 2014; Xu et al., 2019; Hu et al., 2020; Zhao et al., 2020; Wu et al., 2021).

The Fukang Sag (a secondary-order structural unit) is located in the southeastern part of the Central Depression (a first-order structural unit). It is adjacent to the Beisantai Bulge to the east, the Monan Bulge to the west, the southern thrust belt to the south, and the Baijiahai and Mosowan bulges to the north (Figure 1). Its tectonic evolutionary features are closely related to the formation and evolution of peripheral bulge zones, with multiphase stratigraphic overburden developing toward the bulge zone (Xu et al., 2019). Figure 2 shows the Fukang Sag stratigraphic system, including the entire strata from the Carboniferous basement to Quaternary sediments. The target strata of this study are located in the middle and upper Permian, including the Pingdiquan Formation (P_{2p}) and the Shangwuerhe Formation (P_{3w}).

The Shangwuerhe Formation, which is the fill-in deposition during the transition from “foreland” to “depression,” is the study’s focus. A large regional unconformity developed beneath the Shangwuerhe Formation, indicating that it represented the beginning of the unified depressional lacustrine basin. The earliest broadly overlying fan-deltaic deposits were developed in this formation, making it one of the most critical exploration intervals for finding large-scale oil reserves (Xu et al., 2019; Hu et al., 2020).

3 Samples and methods

3.1 Materials and sampling

This paper details the observations on the cores of nine wells drilled in Fukang Sag of Junggar Basin in the last 2 years, with a total length of over 200 m. A total of 150 P_{3w} core samples were collected. Ordinary thin section observation was performed on 70 representative samples, based on which the content of quartz, feldspar, and lithic fragments was classified; the types of lithic fragments were classified; and the structural characteristics (e.g., grain size, sortability, and roundness) and the mode of cementation were analyzed. Approximately 80 samples were prepared into cast thin sections to observe the pore type, morphology, and size and to analyze their relationship with fractures. SEM was applied to 105 samples to observe the filling characteristics of the fillings and pore morphology. Eighteen samples were prepared into thin sections for fluid inclusion analysis.

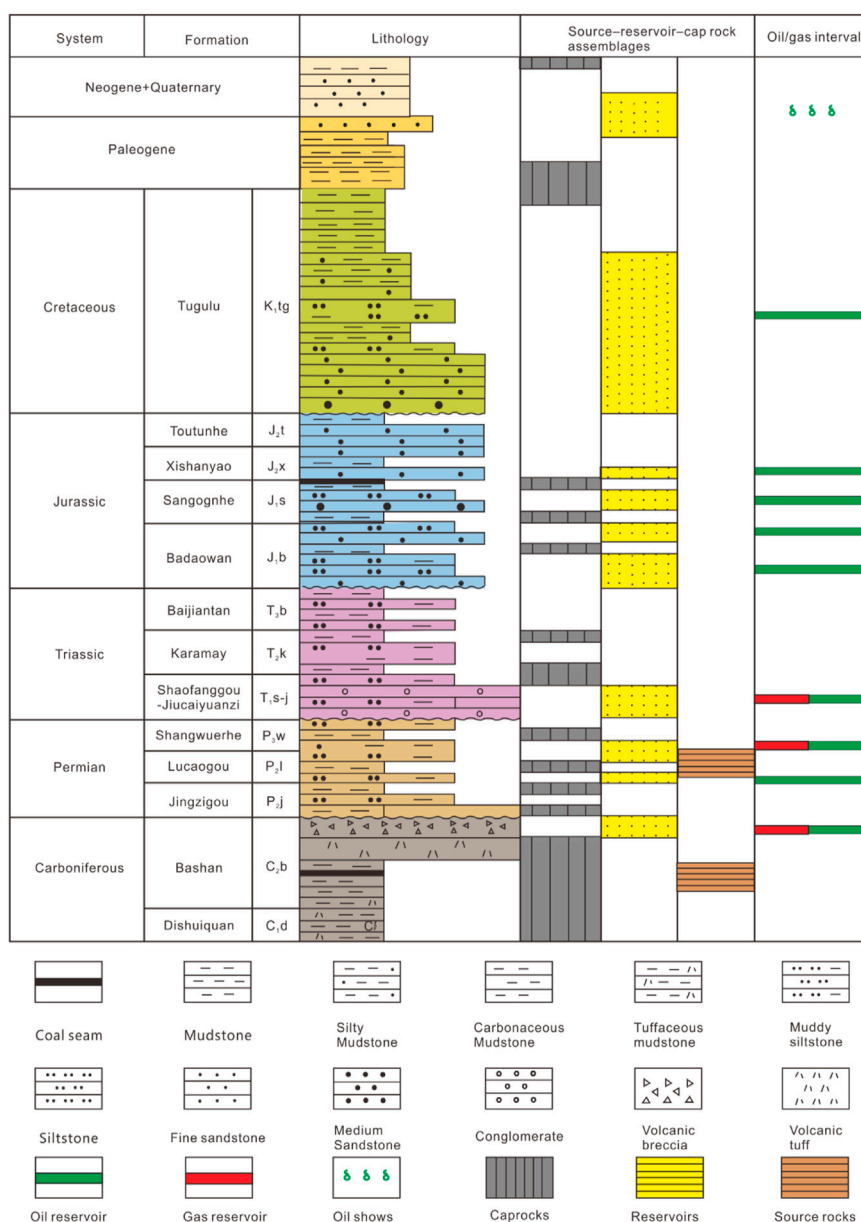


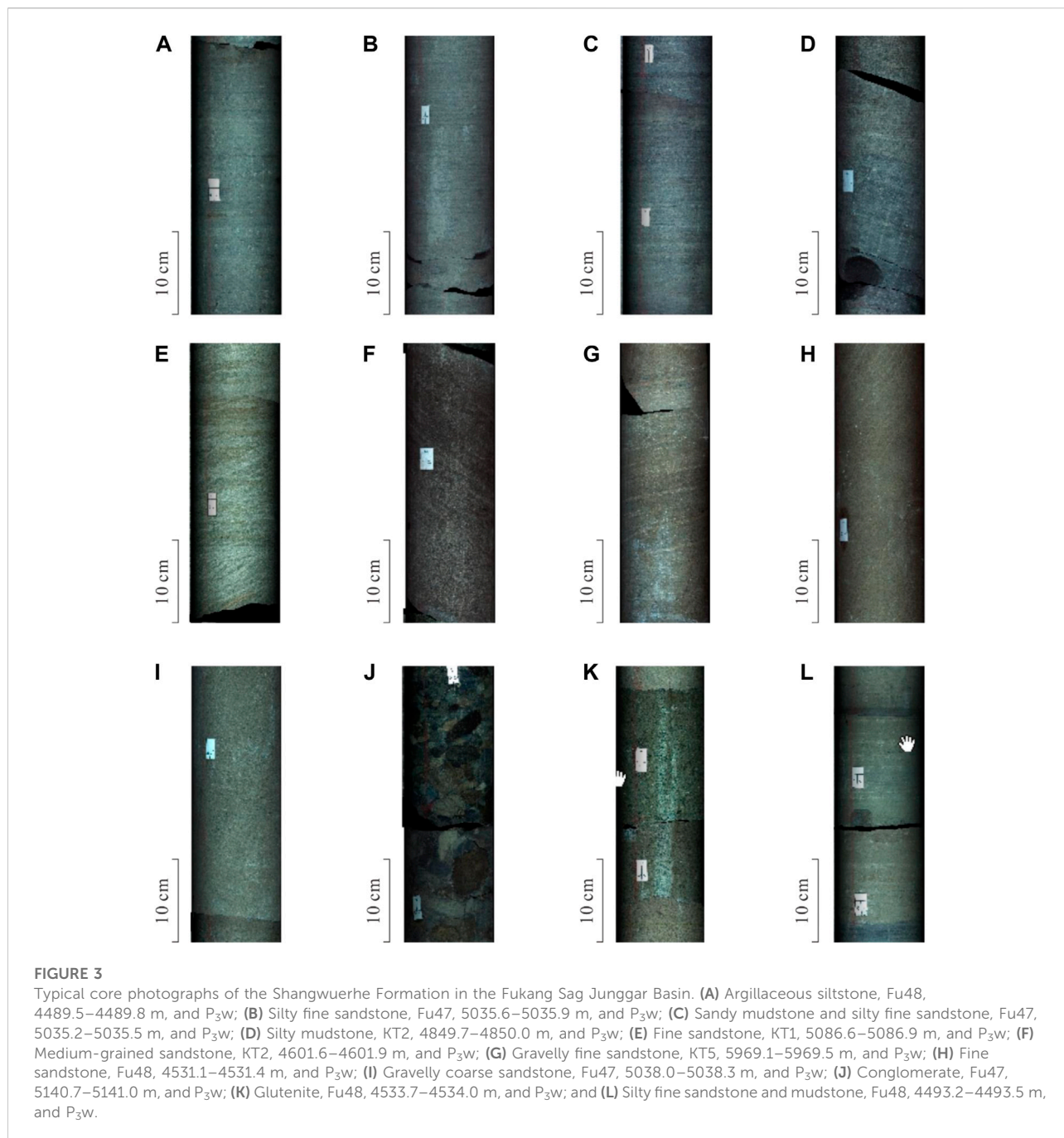
FIGURE 2 Synthetic column of strata, lithology, source rocks, reservoirs, cap rocks, and oil or gas intervals of the Fukang Sag, Junggar Basin (after Gong et al., 2019).

3.2 Mineralogical composition

In this study, the mineralogical composition was obtained following quantitative evaluation of minerals by scanning electron microscopy (QEMSCAN) analysis of cut-out minilet samples (~2 cm²) or random subsamples of each pseudo-cutting interval. Due to the high repeatability of its measurements, QEMSCAN is heavily used in micromineralogy studies, and repeated measurements of the same samples often have more than 98% similarity (Power and Burns, 2013).

3.3 Scanning electron microscopy

In this study, optical microscopy and SEM were combined to observe the morphology and distribution of pores in Fukang samples. Before imaging, both polished and non-polished (freshly crushed) samples were coated with carbon or gold. A smooth surface was obtained by mechanical polishing and, subsequently, ion milling. SEM and energy dispersive X-ray spectroscopy analysis were performed on field-emission scanning electron microscopy (FE-SEM) with an accelerating voltage of 20 kV.

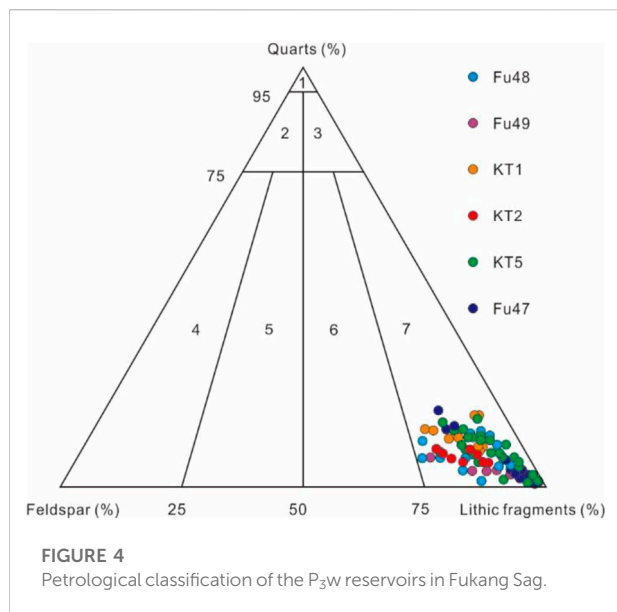


Mercury injection capillary pressure method

High-pressure mercury pore size analysis is a common reservoir pore throat distribution method at the core scale, where liquid mercury (Hg) is injected into the sample. Following the Young-Duper equation, the work required to force mercury into the pores by applied pressure equals the work required to submerge the powder

surface (Roberts et al., 1991). Hence, the specific surface area is obtained, and the average pore radius can be estimated from the pore volume and the specific surface. A high-pressure mercury pore size analysis analyzed pores in the macropore range. The samples must be dried at 110°C for 2 h of free and adsorbed water and vacuumed at low pressure.

All the analytical tests were completed at the Analysis and Testing Center of Xinjiang Oilfield Company, PetroChina.



4 Results

4.1 Reservoir petrology

The P_{3w} clastic reservoirs in the Fukang Sag lithologically comprise argillaceous siltstone, fine sandstone, silty fine sandstone, gravelly fine sandstone, medium-grained sandstone, gravelly coarse sandstone, glutenite, conglomerate, sandy mudstone, and mudstone (Figure 3). Fine sandstone, silty fine sandstone, gravelly fine sandstone, medium-grained sandstone, gravelly coarse sandstone, glutenite, and conglomerate are developed in the distributary channel, underwater distributary channel, and estuary bar sedimentary microfacies. However, argillaceous siltstone and siltstone are developed in distal sand and beach bar microfacies, while sandy mudstone and mudstone are developed in interdistributary bay microfacies and shallow and deep lake subfacies.

Following lithological classification, they are mainly lithic sandstone (or conglomerate) (Figure 4). The quartz content ranges from 1% to 18%, with an average of 6.9%; the feldspar content ranges from 1% to 22%, with an average of 7.6%; and the content of lithic fragments ranges from 68% to 100%, with an average of 85.5%. The quartz particles are not only single-crystal quartz from parent granite rock but also polycrystalline quartz from metamorphic rock. The lithic fragments are dominated by tuffaceous volcanic rocks, whose content accounts for above 70% of the lithic fraction, followed by andesite, fayalite, and a few granite lithic fragments (Figure 5). The main types of reservoir fillings are mud, carbonate minerals, silica, and laumontite. Among them, mud is the primary cement, the content is 2%–12%, and the mud composition is mainly chlorite, illite, kaolinite, and illite-

montmorillonite mixed layer. The genesis of mud cement relates to the alteration of volcanic ash fillings. Carbonate minerals are the secondary cement, with approximately 1%–9% content, mainly calcite and a few rhodochrosites. There are two major forms of siliceous cementation. One is a secondary increase in quartz, and the other is filled with microcrystalline quartz in the pores. The laumontite content ranges from 0% to 3%, with low overall content, and its genesis is related to the hydrolytic alteration of volcanic ash (Figure 5). Generally, the reservoir's compositional and textural maturities are low. The lithic particles are often coarse-grained and have poor–medium sorting. The rounding of lithic particles is often angular and sub-angular. Point–line contact was widely observed between particles, indicating that support mode is frequently particle support, followed by few suspension contacts. Calcite is characterized by basal-type cementation, and clay minerals are characterized by porous cementation.

4.2 Types of reservoir space

The common pore P_{3w} clastic reservoirs in the Fukang Sag include residual primary intergranular pores, intergranular dissolved pores of different degrees, intragrain dissolved pores of lithic fragments, feldspar, and quartz, as well as intergranular pores of cement and fractures (Figure 6). The surface porosity of the secondary dissolved pores in this set of clastic reservoirs accounts for over 90% of the total pores. Intergranular dissolved pores are formed by the dissolution of carbonate cement and rigid grain edges based on primary intergranular pores. Therefore, it is difficult to distinguish between residual primary and secondary intergranular dissolved pores. The pores in the study area were categorized into four types, characterized as follows:

(1) Residual primary intergranular pores

Here, the residual primary intergranular pores in the P_{3w} reservoirs are the pores remaining after mechanical compaction, pressure dissolution, and authigenic mineral filling. Such pores are often distributed in the Well Fu43 area, where the primary pores of the P_{3w} Formation reservoir are preserved by the absence of large-scale carbonate and clay cementation between the clastic particles (Figure 6A). Conversely, the primary intergranular pores were poorly developed in the other area due to strong cementation.

(2) Intergranular dissolved pores

This is a unique P_{3w} reservoir pore type in the Fukang Sag, formed by partial or total dissolution of the outer edges of various volcanic rock fragments and feldspar grains and early-

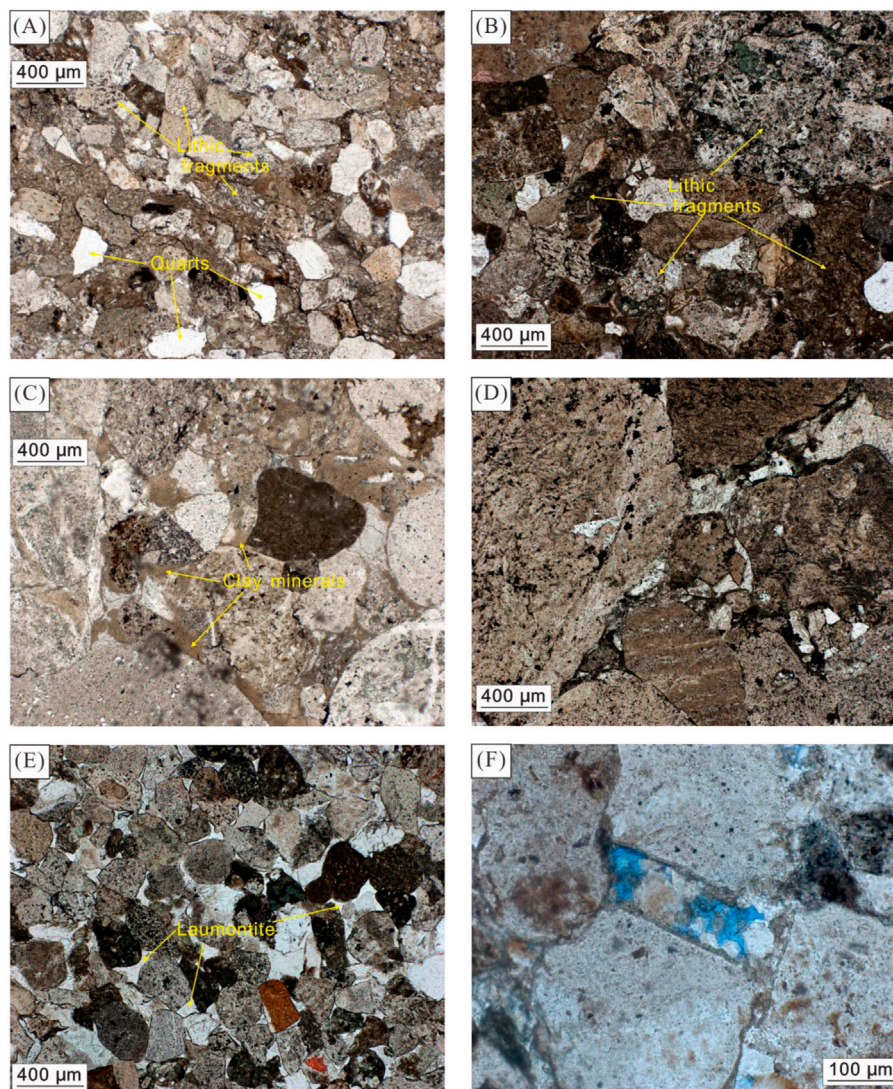


FIGURE 5

Petrological and mineral characteristics of the P_3w reservoirs in Fukang Sag (A) Well Fu48, 4596.1 m, P_3w , fine and medium-grained clastic sandstone, siliceous 3%, and illite-montmorillonite mixed layer 1%; (B) Well Fu47, 5111.3 m, P_3w , gravelly medium-grained clastic sandstone, illite-montmorillonite mixed layer 6%; the reservoir is tight, and the pores are invisible; (C) Well Fu49, 5402.98 m, P_3w , unequal grained sandstone, calcite 2%, and illite-montmorillonite mixed layer 6%; (D) Well KT1, 5161.0 m, P_3w , sandy conglomerate; (E) Well Fu48, 4511.0 m, P_3w , fine-to medium-grained clastic sandstone, laumontite 6%, and a few muddy shrinkage pores were observed; and (F) Well Fu50, 4291.46 m, P_3w , and gravelly medium to coarse-grained clastic sandstone with the intergrain filling of laumontite minerals.

formed carbonate cement. The pore morphology was highly irregular, and harbor-shaped intergranular dissolved pores were observed (Figures 6B,C,E-L). The P_3w reservoir in the study area is tight, and the development of some intergranular dissolved pores is often accompanied by fractures. This indicates that dissolved fluids can only move along the fractures and improve the reservoir around the fractures locally but fail to improve them on a larger scale by penetrating deep into the tight reservoir. During diagenesis, geological fluid enters the reservoir along the fracture. The

surface of soluble mineral particles near the fracture and the calcite cement filled between particles were dissolved first. This dissolution on the surface of particles often cannot completely dissolve minerals. Although the main body of undissolved mineral particles exists in the form of debris, the existence of dissolution distinguishes between intergranular dissolved pores and residual primary intergranular pores.

(3) Intragranular dissolved pores

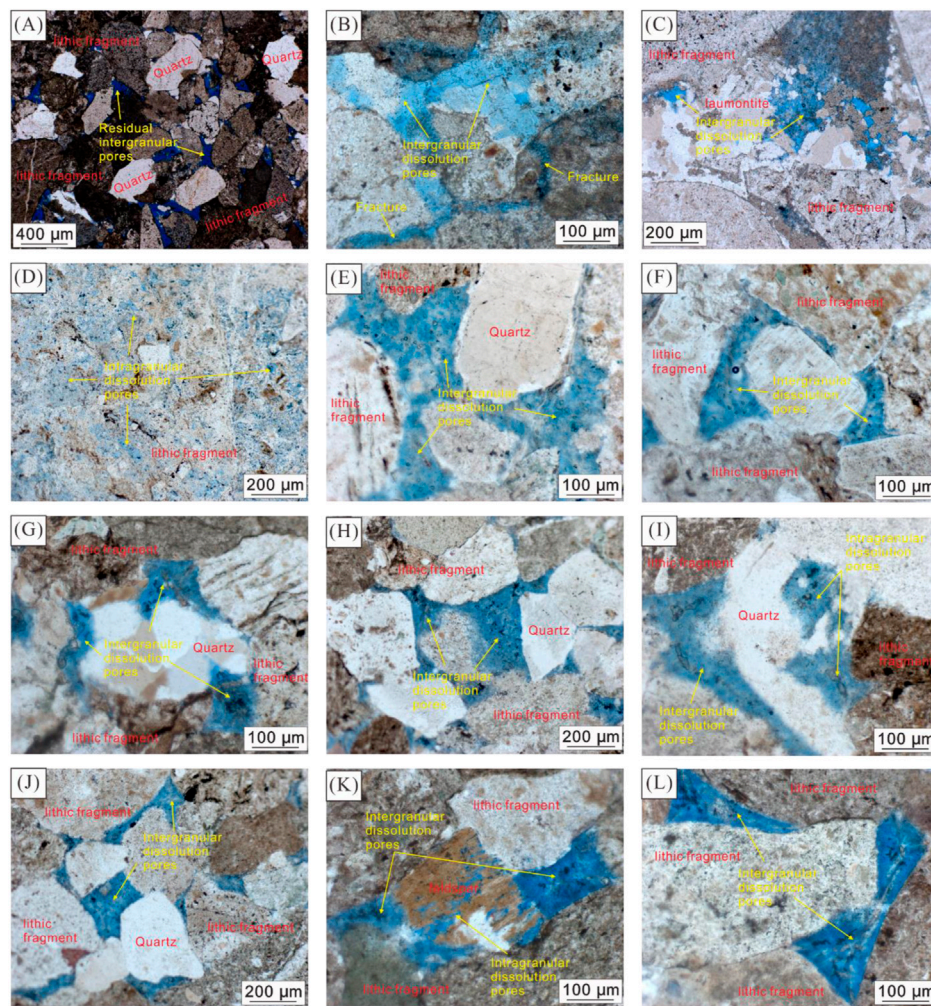


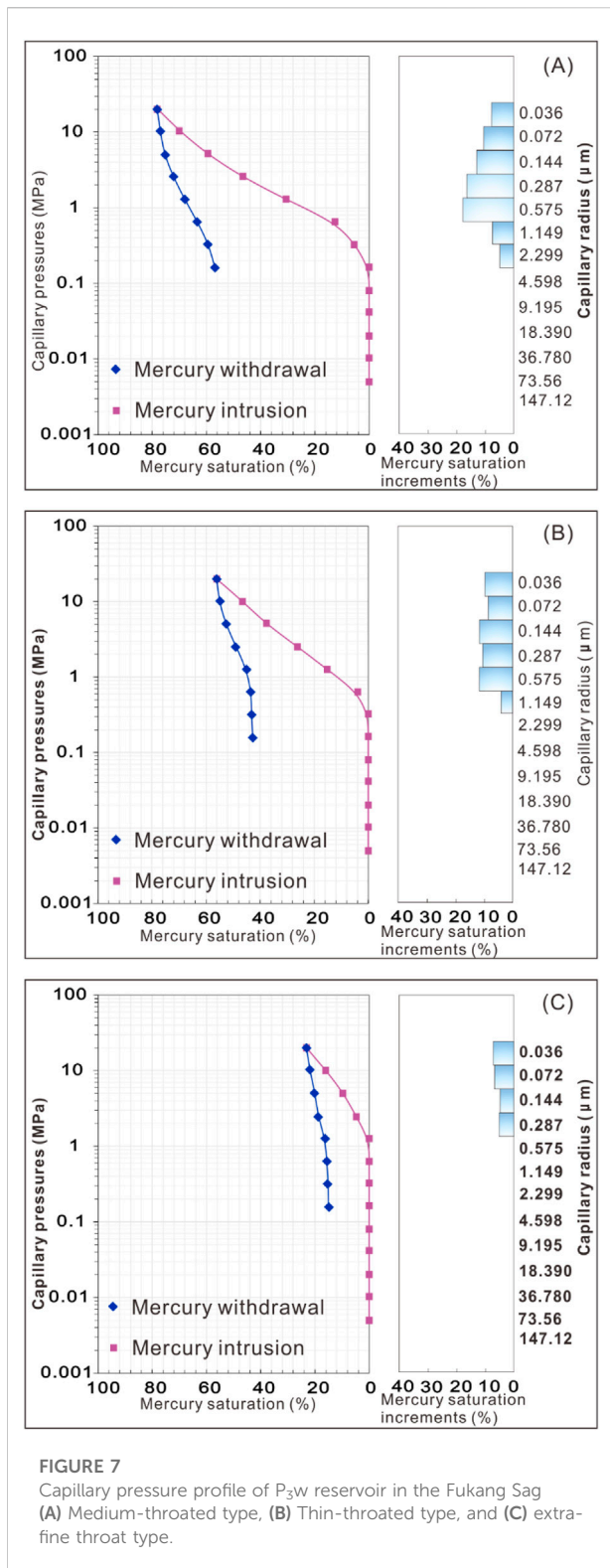
FIGURE 6

Pore characteristics of the P_{3w} reservoir in Fukang Sag under the thin section (A) Well Fu43, 3136.7 m, P_{3w} , and residual intergranular pores; (B) Well KT5, 5944.00 m, P_{3w} , and intergranular pores formed by dissolution of lithic fragments and cement; (C) Well Fu50, 4289.81 m, P_{3w} , and intergranular pores formed by cement dissolution; (D) Well Fu50, 4292.81 m, P_{3w} , and intragranular microporosity formed by dissolution of lithic fragments; (E) Well Fu48, 4541.47 m, P_{3w} , and intergranular pores formed by cement dissolution; (F) Well Fu48, 4541.47 m, P_{3w} , and intergranular pores formed by cement dissolution; (G) Well Fu48, 4541.47 m, P_{3w} , intergranular pore formed by dissolution of polycrystalline quartz, and lithic fragments; (H) Well Fu48, 4541.47 m, P_{3w} , and intergranular pore formed by dissolution of lithic fragments; (I) Well Fu48, 4540.71 m, P_{3w} , and intragranular pores formed by quartz dissolution; (J) Well Fu48 well, 4540.71 m, P_{3w} , and intergranular pores formed by cement dissolution; (K) Well Fu48, 4538.76 m, P_{3w} , intragranular and intergranular pores formed by dissolution of the feldspar and cement; and (L) Well Fu48, 4538.76 m, P_{3w} , and intergranular pores formed by the cement dissolution.

Intragranular dissolved pores are another primary pore type in the P_{3w} reservoirs, formed through the internal dissolution of various rock fragments and feldspar grains (Figures 6D,I,K). Intragrain pore shapes vary from particle to particle, with various types. The lithic fragments could form either intragrain micropores or large pores in continuous distribution. Conversely, the intragrain feldspar pores tend to develop along the decomposition and thus have good connectivity with intergrain pores. The main difference between intragranular dissolved pores and intergranular dissolved pores is that dissolution occurs inside the mineral

particles rather than on the surface, so the pores formed by dissolution are inside mineral particles, and the external contour of mineral particles is unchanged. The formation of intergranular dissolved pores requires minerals to provide a channel for geological fluids to enter inside the particles. Volcanic lithic fragments with a reticular pore structure and feldspar particles with cleavage meet this condition. Thus, they are the main minerals for developing intergranular dissolved pores in the study area.

(4) Fractures



Fractures are moderately developed in the P_{3w} reservoir (Figure 6B), and both tectonic and diagenetic seams can be observed. The pore space of the fractures contributes less to

the reservoir pore space. However, it provides a channel for moving the dissolved fluids, improving the reservoir pore space and significantly enhancing the reservoir permeability in the study area.

4.3 Structural characteristics of the pore throat

The pore structure characteristics refer to the geometry, size, distribution, connectivity, configuration relationship, and evolutionary characteristics of the pores and the throat connected. Pores and throats determine the reservoir space of clastic rocks. Pores affect porosity, and throats affect permeability. Therefore, studying the spatial distribution characteristics and collocation relationship between pores and throats is crucial. The capillary pressure curve pattern and the related parameters of the P_{3w} reservoir in the Fukang Sag were analyzed to discuss the pore throat diameter, connectivity, distribution, and inter-configuration relationship of the reservoir. The pore structure is divided into three types.

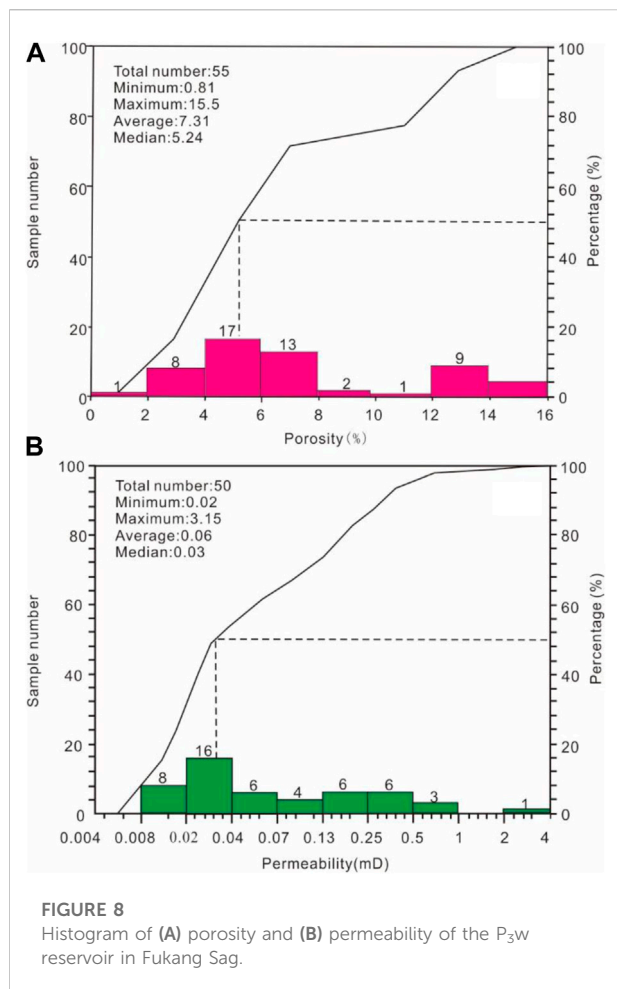
(1) Mid-throat type.

This pore structure accounts for a low proportion in the P_{3w} reservoir in Fukang Sag and is mainly distributed in a few sections in the Wells KT1, KT2, and Fu48 (Figure 7A). A slightly developed platform characterizes its capillary pressure profile and medium pore throat sorting with an average throat radius, median mercury saturation radius, throat sorting coefficient, pore discharge pressure, median mercury saturation pressure, maximum incoming mercury saturation, and mercury withdrawal efficiency of 0.63 μm, 0.23 μm, 2.03, 0.32 Mpa, 6.26 Mpa, 77.88%, and 26.79%, respectively (Figure 7A). The corresponding ranges of porosity and permeability are 13.9–15.5% and 0.69–3.15 mD.

(2) Fine throat type

This is the second type of pore structure in the P_{3w} reservoirs distributed in some sections of the Wells KT1, KT2, Fu47, Fu48, Fu49, and Fu50 (Figure 7B). Its capillary pressure curve is characterized by an inconspicuous plateau and poor pore throat sorting, with an average throat radius, median mercury saturation radius, throat sorting coefficient, pore discharge drive pressure, median mercury saturation pressure, maximum incoming mercury saturation, and mercury withdrawal efficiency of 0.31 μm, 0.05 μm, 1.82, 0.69 Mpa, 13.97 Mpa, 56.15%, and 23.45%, respectively. The corresponding ranges of porosity and permeability are 5.8%–13.3% and 0.04–0.62 mD.

(3) Extra-fine throat type



This is the most dominant pore structure in the P_{3w} reservoir in the Fukang Sag and is widely developed all over the P_{3w} reservoirs in Wells KT1, KT2, KT5, Fu47, Fu48, Fu49, and Fu50 (Figure 7C). The features of its capillary pressure curve are zero platforms, extremely poor pore throat sorting, an average throat radius of approximately 0.1 μm, and a throat sorting coefficient of 0.94. The features also include pore discharge drive pressure greater than 1.0 Mpa, maximum incoming mercury saturation of approximately 23.39%, and mercury withdrawal efficiency of 35.41%. The corresponding range of porosity and permeability are 0.8%–10.4% and 0.01–0.27 mD.

4.4 Physical characteristics of the reservoir

The porosity of the P_{3w} reservoir in Fukang Sag ranges from 0.81% to 15.5%, with average and median values of 7.31% and 5.24%, respectively. The permeability of the P_{3w} reservoir ranges from 0.02 to 3.15 mD, with average and

median values of 0.06 and 0.03 mD, respectively (Figure 8). In the plane, the physical properties of the P_{3w} reservoir of Well KT2 in the southern Fukang subsag are relatively good, with average porosity and permeability of 12% and 0.26 mD, respectively. Conversely, those of Wells Fu47, Fu48, Fu47, and KT2 in the middle Fukang subsag are relatively poor, with average porosity and permeability of 6.02% and 0.07 mD, respectively.

5 Discussion

5.1 Mechanisms of reservoir densification

5.1.1 Carbonate cementation

Carbonate cement is developed in the P_{3w} reservoir in Fukang Sag (Figures 9A,B,H–J). Calcite is the primary type of carbonate cement in the study area, and several Ca²⁺ and CO₃²⁻ are required for calcite formation. The P_{3w} reservoir in Fukang Sag is rich in volcanic lithic fragments. The hydration of tuffaceous and intermediate–basic volcanic lithic fragments could release many Ca²⁺, accounting for the primary calcite source in the P_{3w} reservoir. The analysis of the correlation between the content of tuffaceous/intermediate–basic volcanic lithic fragments and that of carbonate cement showed that the content of carbonate cement increases first and then decreases with the increase of the content of tuffaceous/intermediate–basic volcanic lithic fragments (Figure 10). From the viewpoint of the cementation type, when the content of tuffaceous/intermediate–basic volcanic lithic fragments is below 55%, the cementation is primarily pore type. Moreover, when they are higher than 55%, the cementation is a compression-embedded type (Figure 10). Due to the high plasticity of tuffaceous/intermediate–basic volcanic lithic fragments, an increase in the content of plastic lithic fragments tended to result in an increase in particle compaction and a larger reduction in original pore space, which causes a decrease in cement content.

The carbon source of calcite cement in the P_{3w} reservoir is deep CO₂-rich hydrothermal fluids. The homogenization temperature of fluid inclusions in the P_{3w} reservoir is concentrated in the range of 120°C–130°C and also has a certain distribution in the temperature range of 110°C–120°C and 120°C–130°C. However, according to the burial history and geothermal gradient evolution in the study area, such a high temperature could not be reached at a depth of 1591.38 m during the normal burial evolution, indicating a tectono-thermal event.

Additionally, the illite content in the study area was significantly higher in wells and sections near the fault where the carbonate cement was well developed than in wells and sections far from the fault where the carbonate cement was poorly developed. Most illites were produced in wispy form,

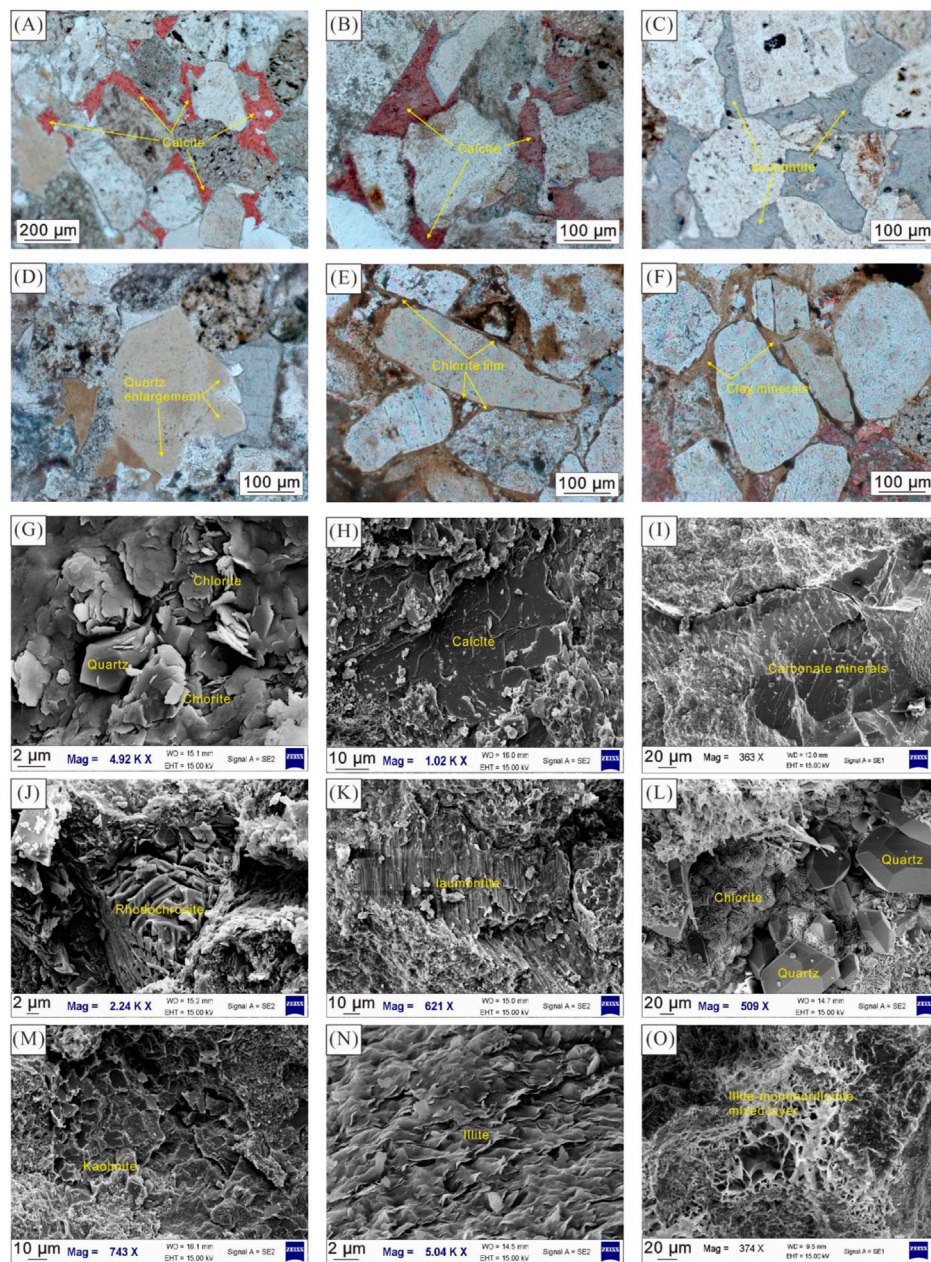


FIGURE 9

Cementation characteristics of the P_3w reservoirs in Fukang Sag (A) Well Fu48, 4492.66 m, P_3w , and calcite cementation; (B) Well Fu49, 5402.69 m, P_3w , and calcite cementation; (C) Well Fu48, 4537.95 m, P_3w , laumontite cementation; (D) Well Fu48, 4471.00 m, P_3w , and secondary enlargement of quartz; (E) Well Fu49, 5384.00 m, P_3w , and clay cementation; (F) Well Fu49, 5384.00 m, P_3w , and intergranular clay-filled; (G) Well Fu47, 5143.60 m, P_3w , intergranular developed granular quartz crystals, and bladed chlorite; (H) Well Fu47, 5038.10 m, P_3w , and intergranularly filled calcite cementation of embedded crystalline; (I) Well Fu49, 5402.69 m, P_3w , and intergranularly filled carbonate minerals; (J) Well Fu48, 4492.36 m, P_3w , and intergranularly filled rhodochrosite cement; (K) Well Fu47, 5135.65 m, P_3w , and intergranularly filled laumontite cement; (L) Well Fu50, 4289.81 m, P_3w , intergranularly filled fluffy chlorite, quartz crystals, and filamentous illite; (M) Well Fu48, 4538.09 m, P_3w , and intergranularly filled book-structure kaolinite; (N) Well KT1, 5085.78 m, P_3w , and intergranularly filled granular illite; and (O) Well KT2, 4602.03 m, P_3w , and intergranularly filled honeycomb-like illite-montmorillonite mixed layer.

and metasomatism of kaolinite was observed (Figures 7O, 9L). The temperature threshold for the conversion of kaolinite to illite is 120°C–140°C. When the temperature exceeds this

threshold, kaolinite converts to illite in large quantities and can form wiry illite (Blanc et al., 2021; Asaad et al., 2022). However, there was an abrupt segment in the study area's

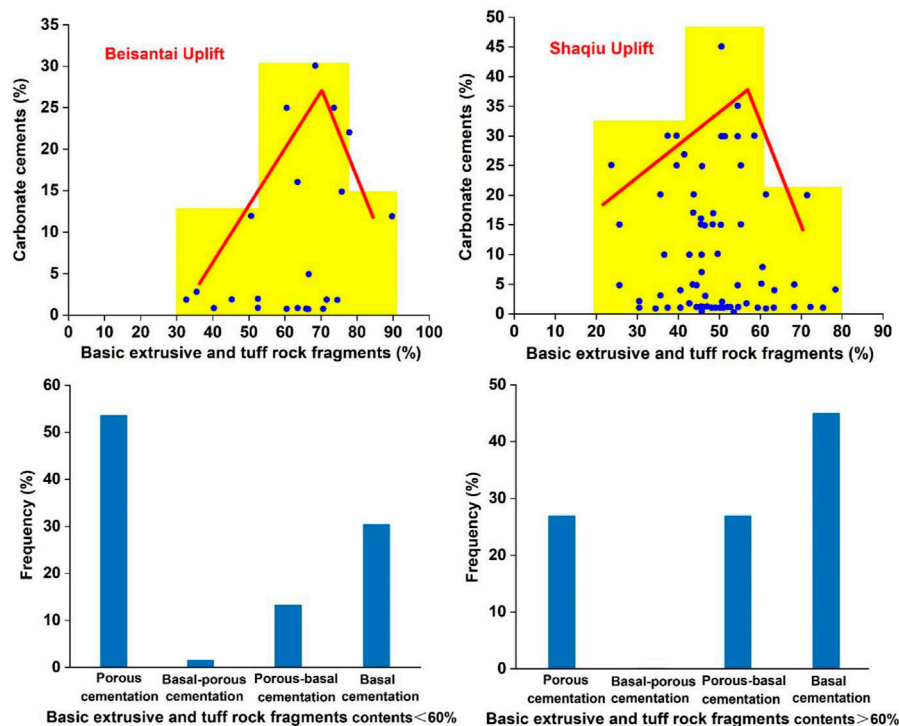


FIGURE 10

Relationships between the content of carbonate cement, the content of volcanic lithic fragments, and the types of cementation in Fukang Sag.

vitrinite reflectance (R_o) profile (Figure 11). Under the consistent tectonic properties of the samples in this area, the intrusion activity of hydrothermal fluid may be the reason for the abrupt change in the R_o profile.

Thus, calcite cement in the P_3w reservoir of Fukang Sag has a deep hydrothermal genesis. The deep hydrothermal fluid moves to the shallow part through the vertical fracture. During this process, the hydrothermal fluid will laterally move along the dominant transport channel (i.e., a highly porous sand body) and react with the rocks. The CO_2 -rich hydrothermal fluid gradually dissolves the feldspar to form the secondary pores during transport and provides several carbon sources, which generate carbonate minerals.

The distribution of calcite in the Fukang Sag is controlled by the content of tuff rock debris and intermediate–basic volcanic rock debris and the distance from the active hydrothermal fault. The average content of calcite corresponds to the distance from the fault and the content of volcanic rock debris. From the perspective of sedimentary facies and lithology, calcite is mainly distributed in fine sandstone, pebbly sandstone, and the conglomerate of those developed at the bottom of underwater distributary channels.

5.1.2 The cementation of chlorite, montmorillonite, and illite

Clay minerals dominate the pore fillings of the P_3w reservoir in the Fukang Sag. This is one of the most critical factors causing the reduction of pore space in deeply buried reservoirs. The main clay mineral types are chlorite, montmorillonite, and illite (Figures 9E–G,L–N). Chlorite is mainly characterized by clay film that develops on the surface of mineral particles. The montmorillonite is honeycomb-like, with many intergranular pores under electron microscopy. However, while the illite demonstrates a lamellar geometry, the intergranular pores are undeveloped.

The montmorillonite in the study area is presumably related to the alteration of pore fillings derived from volcanic ash during the sedimentary period. Several tuffaceous lithic fragments in the sandstone indicate that the source area was rich in volcanic debris during the sedimentary period. The conversion of montmorillonite to illite is an important reaction with two possible mechanisms. In the first mechanism, the Al^{3+} is an active component, while in the second mechanism, the Al^{3+} is inactive. Both reactions require a source of K^+ , obtained from the destruction of clastic potassium feldspar.

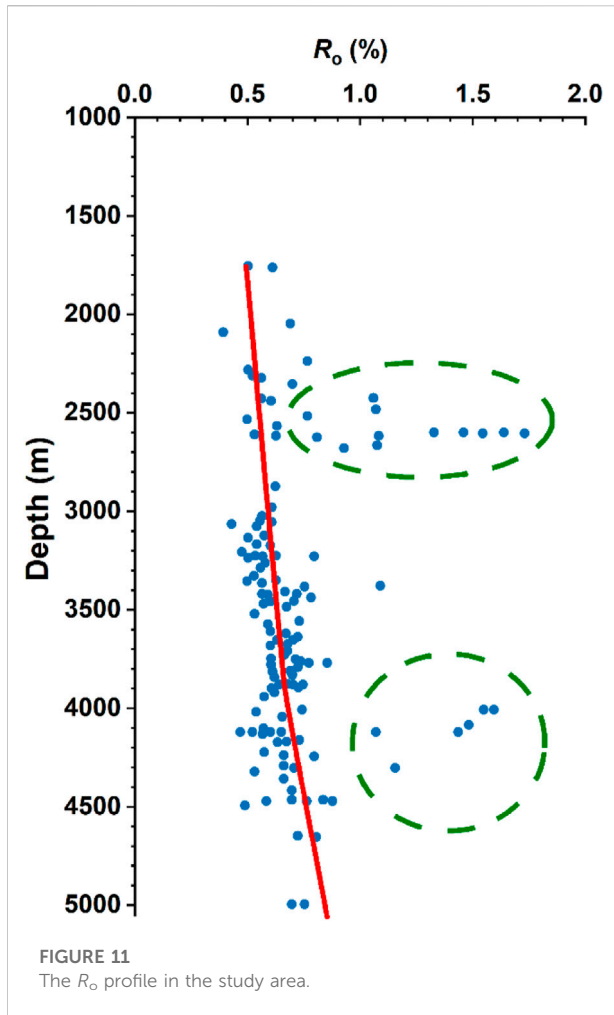
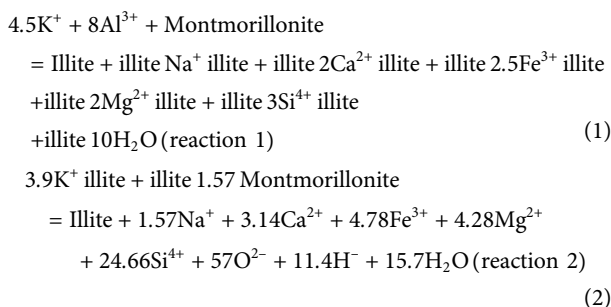


FIGURE 11
The R_o profile in the study area.



For sandstone cementation, the key to the above reaction is the release of various components while converting montmorillonite to illite. These components are found in the diagenetic phase of the P_{3w} reservoir, that is, silica precipitation (Figures 9D,G). The transition from montmorillonite to illite provides significant cement to the reservoir, resulting in great damage.

Particularly, the Si^{4+} released in Reaction two is approximately five times greater than that in Reaction 1, causing the severe quartz cementation observed in the P_{3w} sandstones in the study area. The

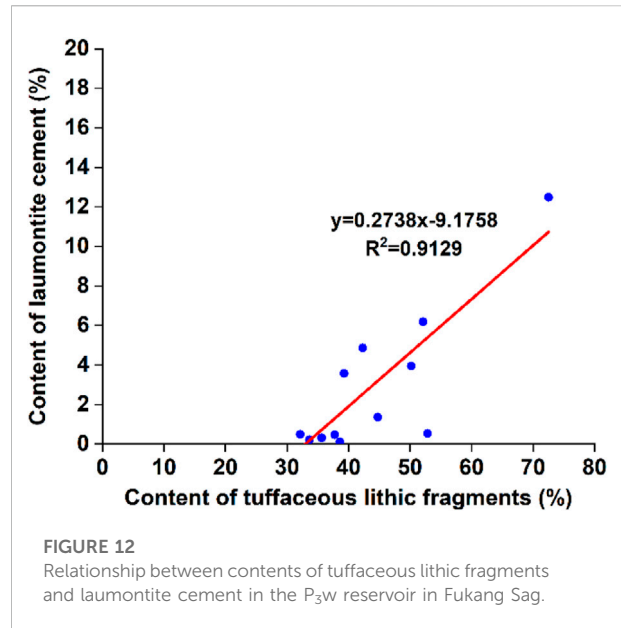


FIGURE 12
Relationship between contents of tuffaceous lithic fragments and laumontite cement in the P_{3w} reservoir in Fukang Sag.

temperature at which montmorillonite starts to convert to illite is more remarkable at around $60^\circ C$ (Blanc et al., 2021; Asaad et al., 2022; Hueck et al., 2022). However, when the temperature exceeds $60^\circ C$ – $100^\circ C$, the silica released from the transitional reaction will be produced in the form of a quartz secondary increase (French and Worden, 2013; Oye et al., 2018; Fiedrich et al., 2020). A secondary enlargement of quartz is developed, and microcrystalline quartz is filled in the pores, combined with several calcite cementations. This indicates that Reaction 2 may be the dominant mechanism of transforming montmorillonite to illite in Fukang Sag.

5.1.3 The cementation of laumontite

The P_{3w} reservoir in Fukang Sag contains some laumontite cement (Figures 9C,K), whose formation mechanisms have two explanations. On the one hand, the formation of laumontite cement relates closely to the development of plagioclase, and laumontite can be formed during the sodic feldsparization of plagioclase. On the other hand, the hydration of tuff material is an important way of forming laumontite. Volcanic tuff contains many unstable minerals at low temperatures, which are rapidly decomposed by hydration and release several K^+ , Na^+ , Ca^{2+} , and Mg^{2+} . This favors the formation of laumontite.

The primary type of clastic rocks in the P_{3w} reservoir is sandstone and conglomerate, with a high content of volcanic lithic fragments and low feldspar content. Thus, the hydration of volcanic tuff material should be the leading cause of the formation of laumontite cement compared with the sodium feldsparization of plagioclase. Using the relationship between the contents of tuffaceous lithic fragments and laumontite cement, a significant positive correlation is observed, indicating that the laumontite starts to appear when the content of the tuffaceous lithic fragments is $>30\%$ (Figure 12).

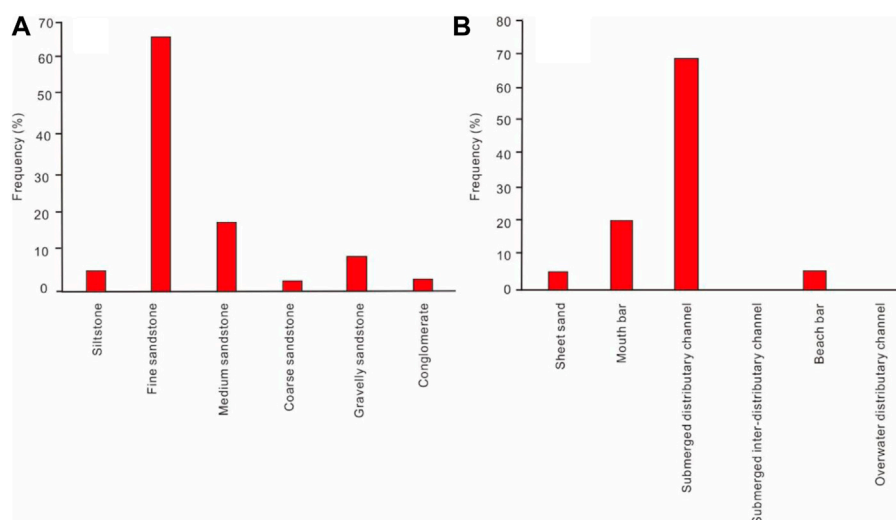


FIGURE 13

(A) Lithology and (B) sedimentary phase of contents of laumontite in the P_{3w} reservoir in Fukang Sag.

Combined with the analysis of single well sedimentary facies, the vertical distribution of laumontite in the study area is discussed. Laumontite cement was distributed mainly in fine sandstone and less in middle sandstone (Figure 13). As for the sedimentary phase, the laumontite is more distributed in the submerged distributary channel microphase and partly in the mouth bar microphase (Figure 13). The depth calibration of laumontite cement from a single well concluded that laumontite cement is mainly formed in the middle and lower parts of the sand body of the submerged distributary channel, with less content at the top (Figure 13).

5.2 The main control factors in forming high-quality reservoirs

The middle-grained sandstone of the Shangwuerhe Formation in Fukang Sag has the highest porosity of 7%–16% and permeability of 0.2–3 mD, followed by siltstone with porosity and permeability of 6%–13% and 0.1–0.2 mD, and fine sandstone with porosity and permeability of 3%–14% and 0.01–0.2 mD. The conglomerate reservoir has the lowest physical properties, with porosity and permeability of 0.5%–7.7% and 0.01–0.05 mD. The higher porosity and permeability of medium sandstone, fine sandstone, and siltstone are mainly related to the higher textural and compositional maturity. Additionally, these rocks contain many soluble mineral components, and the dissolution of soluble minerals by acidic fluids controls the formation of high-quality reservoirs in the study area.

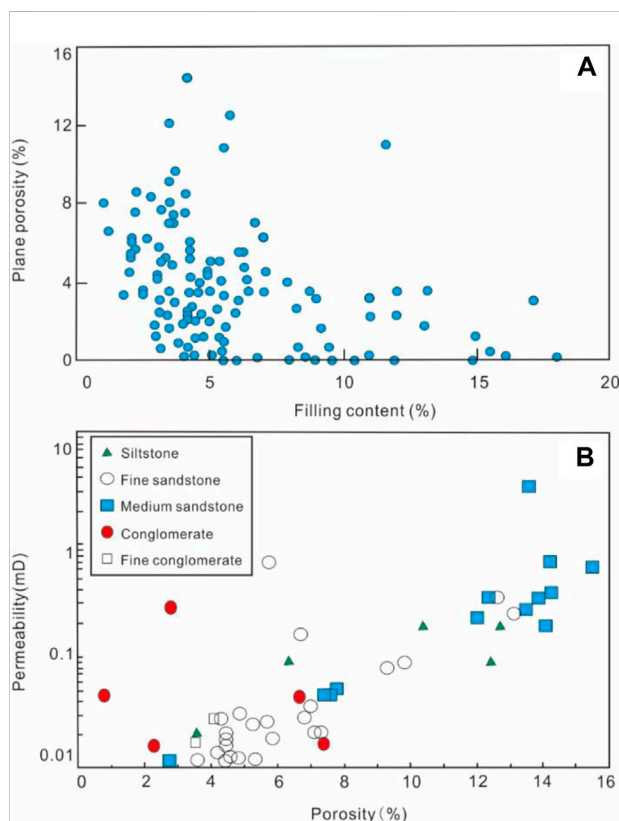


FIGURE 14

The cross plots of (A) plane porosity vs. filling content and (B) porosity vs. permeability of the P_{3w} reservoir in Fukang Sag.

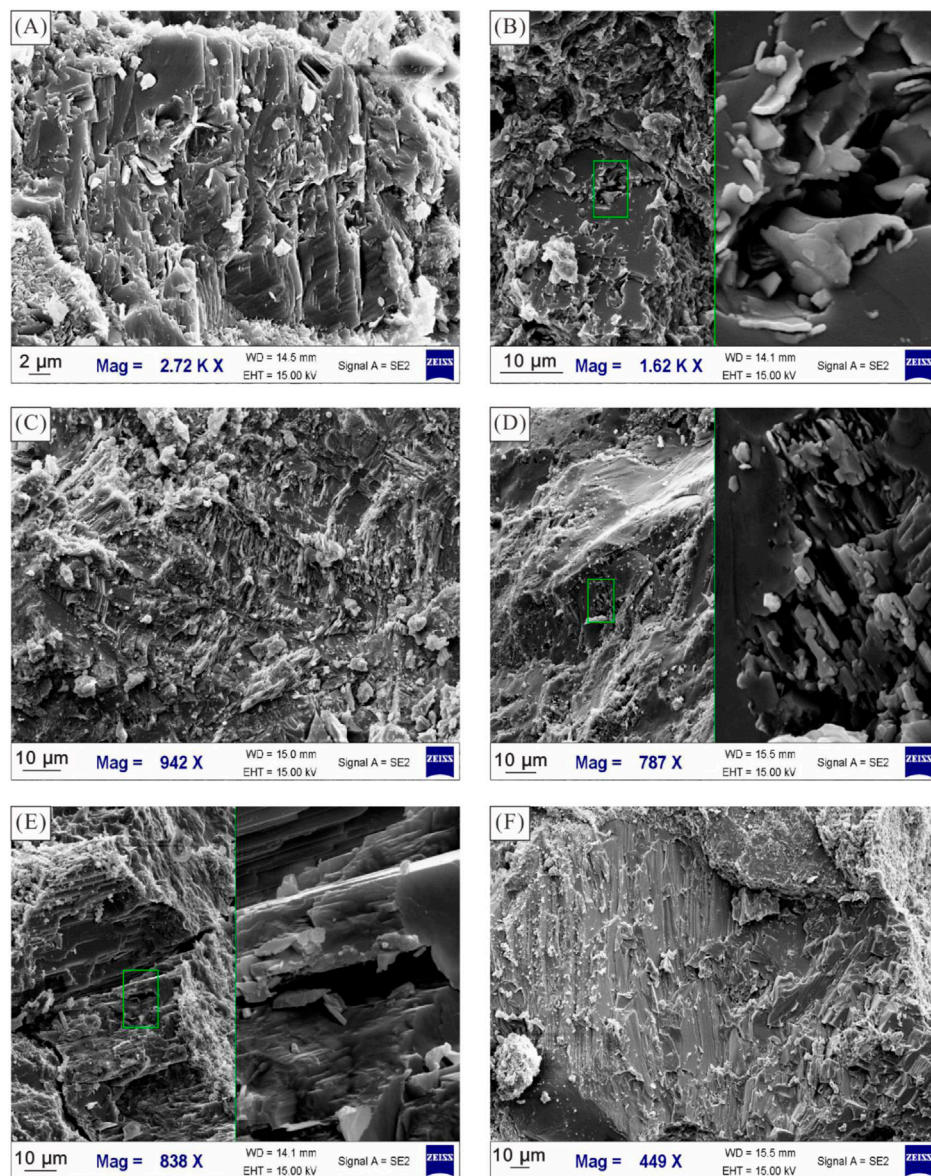


FIGURE 15

Dissolution characteristics of P_3w reservoir in the Fukang Sag (A) Well Fu47, 5128.80 m, P_3w , and grain surface dissolution of feldspar; (B) Well Fu48, 4542.36 m, P_3w , intragrain dissolution of feldspar; (C) Well Fu50, 4179.94 m, P_3w , and intragrain dissolution of lithic fragments; (D) Well Fu47, 5125.2 m, P_3w , and intragrain dissolution of lithic fragments; (E) Well Fu47, 5137.40 m, P_3w , dissolution of laumontite; and (F) Well Fu48, 4540.87 m, P_3w , and dissolution of intergranular calcite.

5.2.1 Influence of rock structure on physical properties

The nature of the parent rock, transport distance, and hydrodynamic conditions determine the composition and structure of the lithic fragments. Sandstones with low matrix content and good sorting have high primary porosity and a slow decay rate of pores and pore throats during diagenesis. In sandstone with high plastic particles and matrix content, the plastic deformation of lithic particles

caused by mechanical compaction can destroy the pore space between particles. The sedimentary environment of the P_3w Formation in Fukang Sag is gradually transitioned from the fan-delta plain to the fan-delta front from the east to the west, and the P_3w reservoirs are mainly sand bodies of distributary channels, submerged distributary channels, and mouth bar. The short transport distances experienced by the sediments result in clastic particles with relatively low compositional and textural maturities but high mud-filling

content. Therefore, the properties of the P_3w clastic reservoir in Fukang Sag are influenced by both filling content and lithology (grain size). From the correlation diagram of surface porosity and filling content, it is observed that surface porosity and filling content are negatively correlated. An increase in the filling content reduces the surface porosity and worsens the reservoir properties (Figure 14). The porosity and grain size correlation plots show that the medium sandstone has better physical properties, while the sand conglomerate has relatively poor physical properties (Figure 14). Summarily, the reservoir's physical properties suit medium sandstone with low clay content and fine sandstone.

Generally, the P_3w reservoir in Fukang Sag is characterized by extra-low pore and extra-low permeability, which corresponds to the depositional environment of the fan-delta. The sandstone reservoir has considerable variation in grain size, poor sorting, and high mud content. Consequently, several muddy matrices were filled between the rock grains, and more intergrain porosity was lost under cementation during the rock formation process, resulting in low permeability and throat radius of the reservoir.

5.2.2 Improvement of reservoir physical properties by dissolution

A comprehensive analysis of the pore type, pore structure, and the relationship between rock-forming minerals and pores illustrated that dissolution is the most significant diagenesis for improving the physical properties of the P_3w reservoir. The surface porosity of dissolution pores accounted for over 90% of the total pores. Dissolution increases the porosity of the reservoir by about 5%–8%. According to the rock thin section, cast thin section, and scanning electron microscope observation, the dissolution phenomenon was observed in several sections of the P_3w reservoir in the study area, mainly characterized by the dissolution of feldspar, lithic fragments, and laumontite (Figure 15). The boundary of the feldspar was dissolved into a harbor shape. Some of the intergranular cement of laumontite showed substantial dissolution, and some showed no dissolution. These nondissolution laumontites are the second phase of laumontite cement formed after the dissolution of early laumontite. Additionally, a few calcite cements were dissolved in the study area. However, it is not widespread and is only seen in some sections of individual wells. The physical properties of these deep reservoirs where the dissolution of calcite cement has occurred have improved, with increased porosity and permeability. No dissolution was seen in most of the core samples drilled in the study area, probably because the reservoir had undergone strong cementation of carbonate, clay, siliceous, and laumontite, and no fractures were developed for acidic fluids to enter into the tight reservoir, thus preventing extensive dissolution of soluble components. Consequently, the P_3w

reservoir in this area is characterized by extremely low porosity and permeability.

6 Conclusion

- (1) The rock type of the clastic P_3w reservoir in Fukang Sag is mainly lithic sandstone and lithic conglomerate. There are two quartz types in the rock component (i.e., single-crystal quartz and polycrystalline quartz). The lithic fragments were derived from tuffaceous volcanic rock and the pore fillings and are composed of clay, carbonate minerals, silica, and laumontite, among others. The reservoir's compositional and textural maturities were poor–medium-sorted, with a roundness of angularity–sub-angularity.
- (2) The physical properties of the P_3w reservoir are characterized by extra-low porosity and extra-low permeability. The P_3w reservoir's porosity ranges from 0.81% to 15.5%, while its permeability mainly ranges from 0.02 to 3.15 mD. The pore types are mainly intergrain dissolved pores and intragrain dissolved pores of lithic fragments, feldspar, and quartz to different degrees. The throat channel is of extra-fine throat type, and the characteristics of the capillary pressure curve are non-platform-type, extremely poor pore throat sorting with an average throat radius of approximately 0.1 μm , and pore discharge pressure of over 1.0 Mpa.
- (3) Calcite, chlorite, montmorillonite, illite-montmorillonite mixed layer, siliceous, and laumontite cementation cause the tight P_3w reservoir in the Fukang Sag. Several Ca^{2+} released by the hydration of tuffaceous lithic fragments and intermediate–basic volcanic lithic fragments in the reservoir and the hydrothermal fluid from deep CO_2 -rich layers trigger the massive development of leucogranite calcite. The formation of several montmorillonites in the fillings is related to the alteration of volcanic tuff fillings during the deposition period in the study area. The hydration of volcanic tuff material triggers laumontite in the P_3w reservoir.
- (4) The properties of the P_3w reservoir are influenced by filling content and lithology, and a negative relationship was observed between surface porosity and filling content. Medium sandstone with low mud content and some fine sandstone reservoirs have the best physical properties. Therefore, the reservoir's physical properties improved the study area due to the dissolution and alteration of calcite, feldspar, and various lithic fragments by acidic fluids.

Data availability statement

The raw data supporting the conclusion of this article will be made available by the authors, without undue reservation.

Author contributions

ZQ: Conceptualization, resources, project administration
 YT: Writing original draft, formal analysis QC: Investigation,
 data curation CL: Investigation, data curation, figure
 preparation HR: Investigation, data curation, figure
 preparation.

Funding

This research is supported by the Prospective and
 Fundamental Project of PetroChina (2021DJ0405).

References

- Asaad, A., Hubert, F., Dazas, B., Razaftianamaharavo, A., Brunet, J., Glaus, M. A., et al. (2022). A baseline study of mineralogical and morphological properties of different size fractions of illite du Puy. *Appl. Clay Sci.* 224, 106517. doi:10.1016/j.clay.2022.106517
- Blanc, P., Gherardi, F., Vieillard, P., Marty, N. C. M., Gailhanou, H., Gaboreau, S., et al. (2021). Thermodynamics for clay minerals: Calculation tools and application to the case of illite/smectite interstratified minerals. *Appl. Geochem.* 130, 104986. doi:10.1016/j.apgeochem.2021.104986
- Du, J. H., He, H. Q., Yang, T., Li, J. Z., Huang, F. X., Guo, B. C., et al. (2014). Progress in China's tight oil exploration and challenges. *China Pet. Explor.* 19 (1), 1–9. (in Chinese with English abstract). doi:10.3969/j.issn.1672-7703.2014.01.001
- Du, J. H., Yang, T., Li, X., Amp, P., and Company, P. (2016). Oil and gas exploration and discovery of PetroChina Company limited during the 13th Five-Year plan and the prospect during the 13th five-year plan. *China Pet. Explor.* 21 (2), 1–15. (in Chinese with English abstract). doi:10.3969/j.issn.1672-7703.2016.02.001
- Du, J. H., Zhi, D. M., Tang, Y., Jia, C. M., Xu, Y., Abulimity, Y. M., et al. (2019). Prospects in upper permian and strategic discovery in shawan sag, Junggar Basin. *China Pet. Explor.* 24 (1), 24–35. (in Chinese with English abstract).
- Fiedrich, A. M., Heinrich, C. A., and Bachmann, O. (2020). Evolution from magmatic to hydrothermal activity beneath the Cerro Escorial volcano (NW Argentina) as sampled by erupted quartz and brines. *Lithos* 374–375, 105706. doi:10.1016/j.lithos.2020.105706
- French, M. W., and Worden, R. H. (2013). Orientation of microcrystalline quartz in the Fontainebleau Formation, Paris Basin and why it preserves porosity. *Sediment. Geol.* 284–285, 149–158. doi:10.1016/j.sedgeo.2012.12.004
- Gong, D. Y., Li, J. Z., Ablimit, I., He, W. J., Lu, S., Liu, D. G., et al. (2018). Geochemical characteristics of natural gases related to Late Paleozoic coal measures in China. *Mar. Petroleum Geol.* 96, 474–500. doi:10.1016/j.marpetgeo.2018.06.017
- Gong, D. Y., Song, Y., Wei, Y. Z., Liu, C. W., Wu, Y. W., Zhang, L. J., et al. (2019). Geochemical characteristics of Carboniferous coaly source rocks and natural gases in the Southeastern Junggar Basin, NW China: Implications for new hydrocarbon explorations. *Int. J. Coal Geol.* 202, 171–189. doi:10.1016/j.coal.2018.12.006
- Gong, D. Y., Wang, Y., Yuan, M., Liu, C. W., Mi, J. L., Lu, S., et al. (2017). Genetic types and origins of natural gases from eastern Fukang Sub-depression of the Junggar Basin, NW China: Implication for low-mature coal-derived gases. *J. Nat. Gas Geoscience* 2, 179–189. doi:10.1016/j.jnggs.2017.07.002
- Guo, J. M., Fan, H. L., Zhang, S. Y., Liu, X., Wu, T., Ma, W. Y., et al. (2020). Petrological, He-Ne-Ar and Sr-Nd-Pb geochemical of volcanic rocks constraint on tectonic settings and geodynamic process of the Carboniferous, East Junggar. *J. Nat. Gas Geoscience* 5 (2), 91–104. doi:10.1016/j.jnggs.2020.02.002
- He, H. Q., and Li, J. Z. (2014). PetroChina's oil and gas exploration results, new geological theories and technological achievements since 11th Five-Year plan period. *China Pet. Explor.* 19 (6), 1–13. (in Chinese with English abstract). doi:10.3969/j.issn.1672-7703.2014.06.001
- He, H. Q., Zhi, D. M., Tang, Y., Liu, C. W., Chen, H., Guo, X. G., et al. (2021). A great discovery of well kangtan 1 in the Fukang sag in the Junggar Basin and

Conflict of interest

The authors declare that the research was conducted in the absence of any commercial or financial relationships that could be construed as a potential conflict of interest.

Publisher's note

All claims expressed in this article are solely those of the authors and do not necessarily represent those of their affiliated organizations, or those of the publisher, the editors and the reviewers. Any product that may be evaluated in this article, or claim that may be made by its manufacturer, is not guaranteed or endorsed by the publisher.

its significance. *China Pet. Explor.* 26 (2), 1–11. (in Chinese with English abstract). doi:10.3969/j.issn.1672-7703.2021.02.001

Hou, M. G., Zha, M., Ding, X. J., Yin, H., Bian, B. L., Liu, H. L., et al. (2021). Source and accumulation process of jurassic biodegraded oil in the eastern Junggar Basin, NW China. *Petroleum Sci.* 18, 1033–1046. doi:10.1016/j.petsci.2021.07.010

Hu, S. Y., Wang, X. J., Cao, Z. L., Li, J. Z., Gong, D. Y., and Xu, Y. (2020). Formation conditions and exploration direction of large and medium gas reservoirs in the Junggar Basin, NW China. *Petroleum Explor. Dev.* 47 (2), 266–279. doi:10.1016/s1876-3804(20)60045-3

Hueck, M., Wemmer, K., Ksienzyk, A. K., Kuehn, R., and Vogel, N. (2022). Potential, premises, and pitfalls of interpreting illite argon dates - a case study from the German Variscides. *Earth-Science Rev.* 232, 104133. doi:10.1016/j.earscirev.2022.104133

Jia, C. Z., Pang, X. Q., and Jiang, F. J. (2016). Research status and development directions of hydrocarbon resources in China. *Petroleum Sci. Bull.* 1 (1), 2–23. doi:10.3969/j.issn.2096-1693.2016.01.001

Jia, C. Z., Zhao, W. Z., Zou, C. N., Feng, Z. Q., Yuan, X. J., Chi, Y. L., et al. (2007). Formation and distribution of volcanic hydrocarbon reservoirs in sedimentary basins of China. *Petroleum Explor. Dev.* 34 (3), 257–271. doi:10.1016/s1876-3804(08)60071-3

Li, C., Chen, G. J., Li, X. T., Zhou, Q. S., and Sun, Z. T. (2022). The occurrence of tight oil in the Chang 8 lacustrine sandstone of the Huaqing area, Ordos Basin, China: Insights into the content of adsorbed oil and its controlling factors. *J. Nat. Gas Geoscience* 7, 27–37. doi:10.1016/j.jnggs.2021.11.001

Lian, X. C., Wang, Z. Q., Ye, C., Liu, Z. Q., and Li, S. T. (2011). Pore structure and influencing factors of reservoir of Sangonghe Formation in Baijiahai area. *Junggar Basin. Lithol. Reserv.* 23, 35–39.

Liu, X. Y., Wei, L. B., Liu, B. X., Zhang, L., Guo, W., Zhang, J. W., et al. (2021). Characteristics of natural gas accumulation in the Cambrian weathered crust in southwestern Ordos Basin. *Nat. Gas. Ind. B* 8 (5), 421–430. doi:10.1016/j.ngib.2021.08.001

Oye, O. J., Aplin, A. C., Jones, S. J., Gluyas, J. G., Bowen, L., Orland, I. J., et al. (2018). Vertical effective stress as a control on quartz cementation in sandstones. *Mar. Petroleum Geol.* 98, 640–652. doi:10.1016/j.marpetgeo.2018.09.017

Power, M., and Burns, S. (2013). “The comparison of WEMSCAN and XRD analysis in the mineralogical characterization of unconventional reservoirs: the benefits of an integrated approach,” in *Geoconvention. CSPG CSEG CWLS* (Calgary, AB, Canada).

Roberts, R. J., Rowe, R. C., and York, P. (1991). The relationship between Young's modulus of elasticity of organic solids and their molecular structure. *Powder Technol.* 65 (1), 139–146. doi:10.1016/0032-5910(91)80176-j

Song, J. Y., Chen, T., and Zhang, J. L. (2022). Permian and triassic hydrocarbon migration and accumulation in the cainan area, Junggar Basin, China. *J. Petroleum Sci. Eng.* 210, 109965. doi:10.1016/j.petrol.2021.109965

Sun, P. A., Wang, Y. C., Leng, K., Hui, W. Y., and Cao, J. (2016). Geochemistry and origin of natural gas in the eastern Junggar Basin, NW China. *Mar. Petroleum Geol.* 75, 240–251. doi:10.1016/j.marpetgeo.2016.04.018

Tang, W. B., Zhang, Y. Y., Pe-piper, G., Piper, D. J. W., Guo, Z., and Li, W. (2021). Permian rifting processes in the NW Junggar Basin, China: Implications for the post-accretionary successor basins. *Gondwana Res.* 98, 107–124. doi:10.1016/j.gr.2021.06.005

- Tang, Y., Guo, W. J., Wang, X. T., Bao, H. J., and Wu, H. S. (2019). A new breakthrough in exploration of large conglomerate oil province in Mahu Sag and its implications. *Xinjiang Pet. Geol.* 40 (2), 127–137. (in Chinese with English abstract). doi:10.7657/XJPG20190201
- Wang, X. L., Zhi, D. M., Wang, Y. T., Chen, J. P., Qin, Z. J., Liu, D. G., et al. (2013). *Geochemistry of source rock and petroleum in the Junggar Basin*. Beijing: Petroleum Industry Press. (in Chinese).
- Wu, C. J., Zhang, M. F., Xiong, D. M., Tuo, J. C., Ma, W. Y., and Qian, Y. (2020). Gas generation from Jurassic coal measures at low mature stage and potential gas accumulation in the eastern Junggar Basin, China. *J. Nat. Gas Sci. Eng.* 84, 103692. doi:10.1016/j.jngse.2020.103692
- Wu, X. Z., Zhou, L., Yang, D. S., Qi, X. F., and Li, B. H. (2012). Structure evolution and hydrocarbon accumulation the Beisantai uplift in Junggar Basin. *Chin. J. Geol. Sci. Geol. Sinica* 47 (3), 653–668. (in Chinese with English abstract).
- Wu, Z. J., Han, X. Z., Ji, H., Cai, Y. F., Xue, L., and Sun, S. J. (2021). Mesozoic-Cenozoic tectonic events of eastern Junggar Basin, NW China and their significance for uranium mineralization: Insights from seismic profiling and AFT dating analysis. *Ore Geol. Rev.* 139, 104488. doi:10.1016/j.oregeorev.2021.104488
- Xu, Q. S., Wang, J., Cao, Y. C., Wang, X. T., Xiao, J., and Kashif, M. (2019). Characteristics and evolution of the late Permian “source-to-sink” system of the Beisantai area in the eastern Junggar Basin, NW China. *J. Asian Earth Sci.* 181, 103907. doi:10.1016/j.jseaes.2019.103907
- Yang, Z., and Zou, C. N. (2019). Exploring petroleum inside source kitchen: Connotation and prospects of source rock oil and gas. *Petroleum Explor. Dev.* 46 (1), 181–193. doi:10.1016/s1876-3804(19)30018-7
- Yu, Z. C., Wang, Z. Z., Wang, J., and Li, Z. Y. (2022). Subtle reservoirs and implications for hydrocarbon exploration in terrestrial lacustrine fan-delta deposits: Insights from the triassic baikouquan formation, Mahu sag, Junggar Basin, Western China. *Mar. Petroleum Geol.* 142, 105730. doi:10.1016/j.marpetgeo.2022.105730
- Zhang, L. L. (2011). *Sedimentary facies of wutonggou formation in Beisantai area in Junggar Basin*. Qingdao: China University of Petroleum. (East China) (in Chinese with English abstract).
- Zhang, M. J., Gong, Z., Tan, Z. H., Liu, H., and Yang, M. X. (2021). Study on heat adsorption based on the experiment of coal adsorption of methane by using the weight method. *J. Nat. Gas Geoscience* 6 (4), 245–253. doi:10.1016/j.jnggs.2021.08.002
- Zhang, S. C., Zhang, S. Y., Fang, L. H., Lu, X. C., Guo, H., and Shi, J. A. (2020). Petrological and geochemical constraints on tectonic settings of the late carboniferous-early permian, central junggar, China. *J. Nat. Gas Geoscience* 5 (1), 1–10. doi:10.1016/j.jnggs.2019.12.002
- Zhang, Z. D., Gu, Y. L., Jin, J., Li, E. T., Yu, S., and Pan, C. C. (2022). Assessing source and maturity of oils in the Mahu sag, Junggar Basin: Molecular concentrations, compositions and carbon isotopes. *Mar. Petroleum Geol.* 141, 105724. doi:10.1016/j.marpetgeo.2022.105724
- Zhao, R., Zhang, J. Y., Zhou, C. M., Zhang, Z. J., Chen, S., Stocklic, D. F., et al. (2020). Tectonic evolution of Tianshan-Bogda-Kelameili mountains, clastic wedge basin infill and chronostratigraphic divisions in the source-to-sink systems of Permian-Jurassic, southern Junggar Basin. *Mar. Petroleum Geol.* 114, 104200. doi:10.1016/j.marpetgeo.2019.104200
- Zhao, S. J., Li, S. Z., Liu, X., Suo, Y. H., Dai, L. M., Lou, D., et al. (2014). Intracontinental orogenic transition: Insights from structures of the eastern Junggar Basin between the alтай and tianshan orogens. *J. Asian Earth Sci.* 88, 137–148. doi:10.1016/j.jseaes.2014.03.008
- Zhi, D. M., Song, Y., Zheng, M. L., Qin, Z. J., and Gong, D. Y. (2012). Genetic types, origins, and accumulation process of natural gas from the southwestern Junggar Basin: New implications for natural gas exploration potential. *Mar. Petroleum Geol.* 123, 104727. doi:10.1016/j.marpetgeo.2020.104727
- Zhou, X. X. (2005). Time-space structure of reservoiring elements and hydrocarbon enrichment-concurrently discussing near-source reservoiring. *Oil Gas Geol.* (6), 711–716. (in Chinese with English abstract).
- Zou, C. N., Xu, C. C., Song, J. R., Li, G. H., Tao, S. Z., Zhu, R. K., et al. (2009). formation and distribution of “continuous” gas reservoirs and their giant gas province: A case from the upper triassic xujiahe formation giant gas province, sichuan basin. *Petroleum Explor. Dev.* 36 (3), 307–319. doi:10.1016/s1876-3804(09)60128-2